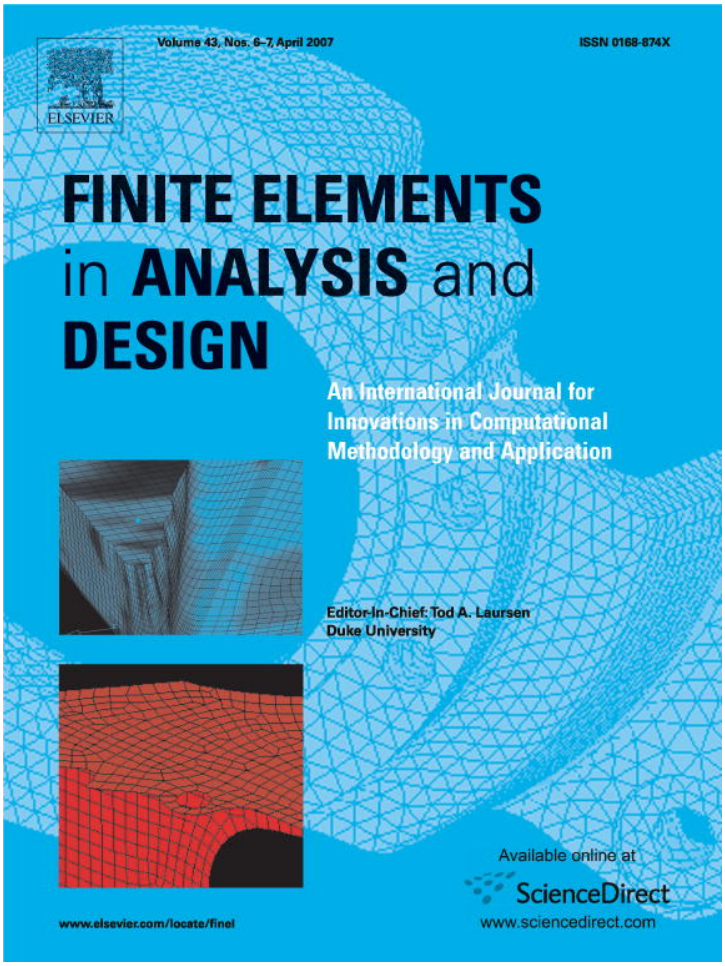

Available online at www.sciencedirect.com
ScienceDirect
Finite Elements in Analysis and Design 43 (2007) 478–493
FINITE ELEMENTS IN ANALYSIS AND DESIGN
www.elsevier.com/locate/finel

Non-uniform isentropic gas flow analysis of explosion in fractured solid media

S. Mohammadi*, A. Pooladi

School of Civil Engineering, University of Tehran, Tehran, IRAN

Received 11 June 2006; received in revised form 5 November 2006; accepted 30 November 2006
Available online 24 January 2007

Abstract

This paper presents a new formulation of non-uniform isentropic gas flow during an explosion in solid media. The present form takes into account additional effects of variations in geometries of voids and crack openings. Variations of mass, density, pressure and internal energy of the gas are analyzed throughout the explosion process, as a means of assessing the feasibility of the adopted approach and verifying the results. The solid material is modeled by a combined finite/discrete element method which is capable of modeling progressive cracking and fragmentation and any potential normal and frictional contacts during the cracking and post-cracking phases. Re-meshing is performed to geometrically model creation/propagation of new cracks or fragments. The proposed algorithm combines the simplicity of the gas flow formulation with the generality of the combined finite/discrete element to achieve a coupled solution for interaction of gas flow and fractured solid in an explosion process. A set of simple classical tests and complex progressive fracturing of a solid domain due to explosion are simulated to assess the overall performance of the proposed approach.

Keywords: Blast; Explosion; Gas–solid interaction; Combined finite/discrete element method

1. Introduction

Engineers have for many years used simplified empirical formulae and sometimes experienced-based rules to design explosive material for achieving a specific engineering goal. These methods have now been replaced by more sophisticated analytical–experimental-based approaches, such as the Kuz-Ram model [1], etc., which combine experimentally supported data within an engineering step by step approach for analyzing the effects of explosions. These are well developed and widely used in rock blasting and tunneling industries which have long been involved with explosive materials and blast effects and hazards.

Extreme pressure and temperature, shock waves, high velocity fragments, very short duration of a blast reaction and chemo-physical characteristics of explosives, are among the important factors that affect both the safety concerns and structural response in an explosion. Despite the complexity of a broad range of effects, fundamental detonation shock wave formulation dates back to the late 19s century [2,3]. Nevertheless, engineering practices have mainly focused on experimental data collected from designed experiments, and observations and measurements of real explosions in wars.

Problems of explosive loading on structures and simulation of the explosion process have recently been re-considered by including all potential coupling and interaction effects; relying on the fast development of computational hardware and availability of efficient numerical algorithms. The long-term goal is now to simulate the whole process of detonation, gas flow, solid deformation and cracking and interaction phenomena in a unified approach.

Continuum mechanics, thermodynamics, gas dynamics, chemistry and physics of explosive material, generation of shock waves, cracking and nonlinear behavior of solid materials, are all coupled in a blast phenomenon. As a result, a comprehensive modeling of explosion would require a fully coupled analysis involving a large variety of different engineering disciplines. This is, however, unlikely to be attainable in

* Corresponding author. Tel.: +98 21 6111 2258; fax: +98 21 6640 3808.
E-mail address: smoham@ut.ac.ir (S. Mohammadi).

0168-874X/$ - see front matter © 2007 Elsevier B.V. All rights reserved.
doi:10.1016/j.finel.2006.11.005

a single unified numerical approach, and therefore, simplified solutions are required. Each simplified approach, which can yet be extremely complex, adopts a numerical approach for decoupling the system or uses experimentally supported formulae as *a priori* assumption for solving a specific part of the approach.

Several blast-induced gas pressure models have been proposed in recent years for simulating the explosion process [4–12]. They include a simple model of a user-defined pressure–time curve without any coupling effect [5], which has been proved to be sensitive to the experience of the user. Munjiza et al. developed a combined finite/discrete element methodology for simulation of progressive fracture in brittle media [6,7]. They used a simple no-flow gas model based on the assumption of a constant pressure in the borehole, which changes with an estimate of the current volume of the borehole at each time. This model is a first step towards coupling the gas flow and solid response.

Other researchers have also reported successful implementation of simplified gas flow interaction with the solid media in simulating rock blasting problems during the past decade using the concepts of hydraulic fracture, discrete element method, etc. [8–14]. Mohammadi et al. [15] has recently reported a two-mesh coupled model based on the flow of gas through an equivalent porous medium. Independent gas and solid meshes are used to solve the governing equations of gas and solid media, respectively. The method indirectly simulates the flow of gas through the crack openings and voids by using the principles of porous mechanics, and the main part of the approach is related to the definition and evaluation of a permeability matrix for the porous medium.

From a different point of view, Munjiza et al. [16,17] proposed a new approach to simulate the gas flow through a cracked medium as a gas flow through uniform pipes. According to the proposed approach, gas characteristics are updated in time based on a uniform frictional gas flow model. Comparable results with available experimental data were also reported. In this method, no independent finite element solution is required to evaluate the gas flow characteristics. Instead, relevant gas dynamics equations have to be solved.

In this paper, the original idea of simplified uniform gas flow [17] is extended to non-uniform isentropic gas flow dynamics and implemented into a combined finite/discrete element algorithm for simulation of a blast in fractured solid. This improves the way different joints and crack openings can be treated while letting the gas flow through. An effective blast zone is also considered for simulating the gas escape from a contained control volume. Gas pressure will only be applied if placed inside a predefined effective zone.

In the following, the main steps of the simulation strategy will be explained. A brief review of the combined finite/discrete element method is also provided. The next section deals with gas–solid interaction models. Then details of the proposed formulation will be provided and discussed. A section of numerical simulations that describes results of the proposed analysis will follow.

2. Modeling strategy

Assume a rock blasting problem that consists of an explosion chamber, also called the borehole, filled with an explosive material (Fig. 1). After detonation, the explosive material is transformed into a high pressure and high density gas. The high pressure acting onto the borehole walls causes deformation and cracking of the solid material followed by fragmentation. The finite/discrete element methodology [9,16–19] has been specifically designed to solve problems involving highly deforming/fracturing media that are accompanied by discontinuities. The part of solid that is susceptible to cracking and fragmentation is modeled by discrete elements, which are classical finite elements empowered by crack propagation and remeshing techniques and contact detection/interaction algorithms, and the rest of the solid is simulated by standard finite elements to avoid contact and fracture computations [18].

Simulation starts by detonation of the explosive material and its conversion to a high pressure and high density gas (Fig. 2a), which is characterized by an equation of state (EOS). The next step is to apply the pressure to the solid medium (Fig. 2b) and to let it deform and fracture (Fig. 2c). This is performed by a combined finite/discrete element procedure. Expansion of the borehole and creation of potential cracks allow for gas expansion and flow through the crack openings, which will consequently reduce gas pressure and density (Fig. 2d). This coupled procedure of gas flow and solid deformation is followed until the gas overpressure vanishes.

Simulation of the fracturing solid medium is based on a central difference explicit time integration analysis within a fully nonlinear combined finite/discrete element approach. At each loading increment, stress states are evaluated from a Rankine softening plasticity model [15]. It also provides measures for estimation of crack initiation or propagation and predicts directions for crack propagations. The procedure then uses a local adaptive re-meshing approach to geometrically model the created cracks and fragments. Special algorithms have to be adopted to transfer state variables from the old mesh to the new one [18], while maintaining equilibrium and consistency conditions.

Adopting nonlinear frictional contact mechanisms is the next step which governs post-cracking interactions among the crack faces or fragments. It enforces normal impenetrability conditions and frictional stick-slip laws to determine post-contact

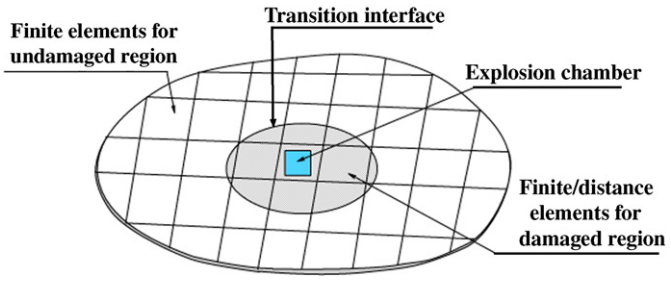

Fig. 1. Combined finite/discrete element model.

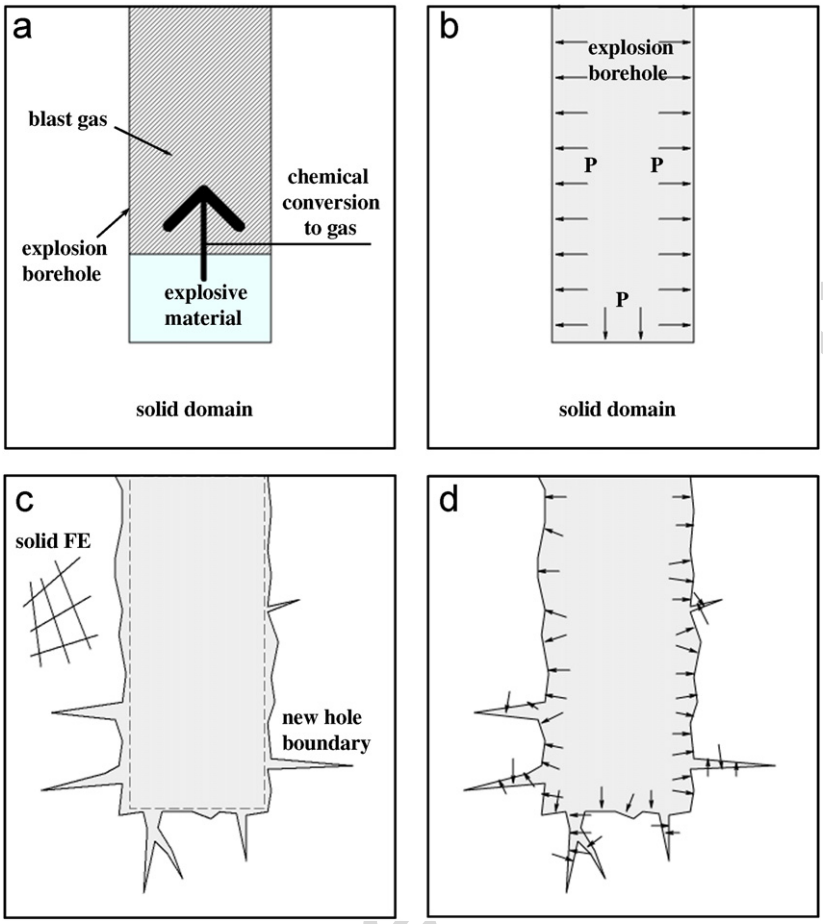

Fig. 2. Three phases of a coupled gas–solid solution. (a) Conversion into blast gas, (b) applying gas pressure on solid, (c) solid deformation and cracking, (d) new gas pressure state on deformed/cracked faces.

displacement and stress states of the interacting bodies. Node to node, node to face, face to face and multiple contact algorithms are required to efficiently simulate all potential interactions between discontinuous objects.

The procedure can be repeated for the remaining load increments. No restriction exists for the number of cracks or fragments to be created.

3. Coupled gas–solid interaction

During a blast in a solid medium, extremely high pressures are rapidly applied to the surrounding medium in a fraction of milliseconds or microseconds, depending on the type of explosive material. Producing extensive deformation and cracking. Gas produced from the blast will then expand and penetrate into the openings and cracks, resulting in a reduction in pressure and internal energy. This is a highly complex interaction phenomenon which has to be addressed.

In earlier approaches, empiric and semi-analytical formulae were embedded within available computational algorithms and finite element software. Their main disadvantage was in adopting a predefined pressure–time curve. These methods can be categorized as non-interaction algorithms. One of the first practical gas–solid interaction models can be attributed to Munjiza [6], who used a simple gas expansion model and an EOS to define variations of pressure in terms of gas density. Others improved the analysis based on the assumption that the gas pressure is constant inside and in the vicinity of the blast hole. It was only a function of hole's volume and its associated crack patterns. The pressure is neglected for the remaining points of the domain. Only one mesh was necessary for numerical modeling.

Other methods based on the gas flow through a porous medium are also available. In this class, the cracked medium is simulated as a porous medium with equivalent properties of density, porosity and permeability [20]. A second independent finite element mesh (g-mesh) is then required to solve the gas flow equation and to couple the results to the solid finite element mesh (s-mesh). A square element FE model has been successfully developed for simulation of blasting process in brittle media [15] (Fig. 3).

The solution is then interconnected to an independent finite element solution of the solid phase. Correlation of the equivalent medium and the real cracked solid medium requires extensive numerical studies and comparisons to available blast data.

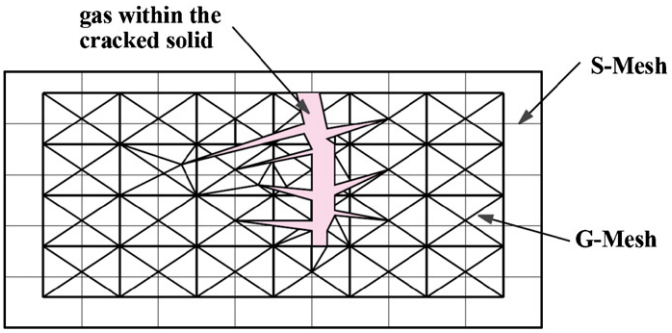

Fig. 3. A two-mesh coupled model. The complex gas chamber is composed of the borehole and cracked solid medium.

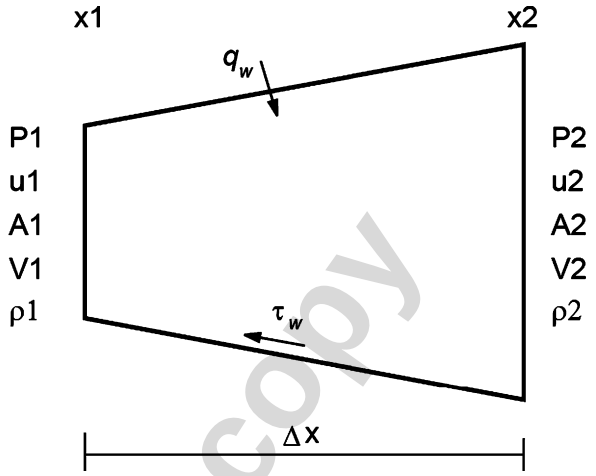

Fig. 4. Flow through a control volume.

In this paper, a new approach based on the definition of an "effective zone" is proposed which avoids the complexity of a coupled two-mesh finite element solutions. It can also be combined with the full coupled two-mesh algorithm, which is the subject of an independent report [21].

3.1. Isentropic gas flow

In a large number of applications, the mass of explosive material and the gas generated by the explosion remain substantially small in comparison to the extent and large mass of the solid material. It is then feasible to assume that the mechanical work of the gas caused by sharp decrease of gas pressure only happens in a small time from the detonation. As a result, the main part of the gas flow can be considered to take place in a region around the explosive borehole.

After detonation, the high pressure gas acting on the walls of the borehole, creates extensive deformation and cracking in solid material, accompanied by expansion, propagation and penetration of the gas into the voids and crack openings. The gas flow can then be divided into two parts: one is associated with the gas flow through existing voids and crack openings, whereas the second part is related to the solid expansion and cracking, reducing the gas pressure and internal specific energy due to the mechanical work.

Gas flow through cracks and openings can now be simulated as a unidirectional flow through an arbitrary shaped conduit/duct. It is important to note that even though solid walls of the duct can freely deform with other parts of the solid domain, however, their motions are relatively slow compared to the rate at which any transient turbulence of detonation gas yield to thermodynamic equilibrium. The reason can be attributed to the much larger mass of the solid than the mass of explosive gas. Thus, at every stage of the deformation, it is assumed that the detonation gas remains in the state of thermodynamic equilibrium.

In order to study the gas flow dynamics, equations of conservation of mass, linear momentum and energy are derived over a control volume of the gas in a so-called Eulerian description. The rate of variation of a typical $\mathbf{X}$ variable over the control volume Ω with the control surface Γ can be defined as [22]

$$\frac{\mathrm{d}\mathbf{X}}{\mathrm{d}t} = \frac{\partial}{\partial t}\int_{\Omega} x\rho \,\mathrm{d}\Omega + \int_{\Gamma} x(\rho V \,\mathrm{d}\Gamma), \tag{1}$$

where x is the value of $\mathbf{X}$ per unit mass, ρ denotes density and V is velocity. Different equations of mass, momentum and energy balance can be derived by setting $\mathbf{X}$ as mass M, linear momentum MV and specific energy of the system e, respectively. The specific energy e is defined as

$$e = u + \tfrac{1}{2}V^2 + gz, \tag{2}$$

where u is the internal energy, g is the gravity acceleration and $z$is the height level from a potential base.

In order to formulate unidirectional gas flow through an arbitrary shaped conduit, a typical control volume is assumed as depicted in Fig. 4. The external heat flux q_{w} through the volume sides is assumed as a constant parameter; a constant friction τ_{w} is also assumed.

The governing mass, momentum and energy conservation equations for a steady gas flow can be derived from (1) by omitting the transient terms, resulting in

$$\begin{aligned} &V\frac{\mathrm{d}\rho}{\mathrm{d}x} + \rho\frac{\mathrm{d}V}{\mathrm{d}x} = -\frac{\rho V}{A}\frac{\mathrm{d}A}{\mathrm{d}x},\\ &\rho V\frac{\mathrm{d}V}{\mathrm{d}x} + \frac{\mathrm{d}P}{\mathrm{d}x} = -\frac{\tau_{\mathrm{w}} l}{A},\\ &\frac{\mathrm{d}P}{\mathrm{d}x} - c^2\frac{\mathrm{d}\rho}{\mathrm{d}x} = \frac{(q_{\mathrm{w}} + \tau_{\mathrm{w}} V)l}{\rho V A\,(\partial u/\partial P)|_{\rho}} \end{aligned} \tag{3}$$

or in a matrix form,

$$\begin{bmatrix} V & \rho & 0\\ 0 & \rho V & 1\\ -c^2 & 0 & 1 \end{bmatrix} \begin{bmatrix} \dfrac{\mathrm{d}\rho}{\mathrm{d}x}\\ \dfrac{\mathrm{d}V}{\mathrm{d}x}\\ \dfrac{\mathrm{d}P}{\mathrm{d}x} \end{bmatrix} = \begin{bmatrix} -\dfrac{\rho V}{A}\dfrac{\mathrm{d}A}{\mathrm{d}x}\\ -\dfrac{\tau_{\mathrm{w}} l}{A}\\ \dfrac{(q_{\mathrm{w}} + \tau_{\mathrm{w}} V)l}{\rho V A(\partial u/\partial P)|_{\rho}} \end{bmatrix}, \tag{4}$$

where A is the cross section area of the duct, P is the pressure and c is the speed of sound for an ideal gas

$$c^2 = \left(\frac{\partial P}{\partial \rho}\right)_s = \gamma RT. \tag{5}$$

Eq. (4) can be solved to give

$$\frac{\mathrm{d}\rho}{\mathrm{d}x} = \frac{1}{A}\frac{-\rho V^2 \mathrm{d}A/\mathrm{d}x + \tau_w l + (q_w + \tau_w V)\, l/\rho V(\partial u/\partial P)|_\rho}{(V^2 - c^2)}, \tag{6}$$

$$\frac{\mathrm{d}V}{\mathrm{d}x} = \frac{1}{A}\frac{c^2\rho V \mathrm{d}A/\mathrm{d}x - V\tau_w l - (q_w + \tau_w V) l/\rho(\partial u/\partial P)|_\rho}{\rho(V^2 - c^2)}, \tag{7}$$

$$\frac{\mathrm{d}P}{\mathrm{d}x} = \frac{1}{A}\frac{-c^2\rho V^2 \mathrm{d}A/\mathrm{d}x + c^2\tau_w l + (q_w + \tau_w V) lV/\rho(\partial u/\partial P)|_\rho}{(V^2 - c^2)}. \tag{8}$$

3.2. Isentropic expansion

Assume an explosion within a thermally isolated chamber with non-rigid walls. If the chamber is filled with gas, the gas will expand in a reversible thermo dynamical process. Therefore, only the mechanical work of gas pressure contributes to the change of internal energy

$$\mathrm{d}u = -P\,\mathrm{d}v \tag{9}$$

where $v = 1/\rho$ is the specific volume. By assuming that variation of the internal energy is only a function of gas temperature,

$$\mathrm{d}u = C_v\,\mathrm{d}T, \tag{10}$$

$$C_v = \left(\frac{\partial u}{\partial T}\right)_v. \tag{11}$$

results in,

$$C_v\,\mathrm{d}T = -P\,\mathrm{d}v. \tag{12}$$

In order to further proceed with the formulation, the following general form of the EOS is considered:

$$P = (\rho + a\rho^b)RT, \tag{13}$$

where a and b are material constants. No fundamental changes are required if other forms of the EOS are adopted. Eq. (13) can also be used to determine the characteristics of gas at an earlier stage of the explosion where the gas simply expands to fill the chamber without any deformation of chamber walls. Eq. (12) can be combined with (13) to give

$$C_v\,\mathrm{d}T = -(\rho + a\rho^b)RT\,\mathrm{d}v \tag{14}$$

with the help of $\mathrm{d}v = -(1/\rho^2)\mathrm{d}\rho$,

$$\frac{C_v}{R}\frac{\mathrm{d}T}{T} = \left(\frac{1}{\rho} + a\rho^{b-2}\right)\mathrm{d}\rho. \tag{15}$$

Integrating from an initial state (subscript $_0$) to the current state results in

$$\int_{T_0}^{T}\frac{1}{T}\,\mathrm{d}T = \int_{\rho_0}^{\rho}\frac{R}{C_v}\left(\frac{1}{\rho} + a\rho^{b-2}\right)\mathrm{d}\rho. \tag{16}$$

With the final solution using the new definition $\gamma = R/C_v + 1$

$$\frac{T}{T_0} = \left(\frac{\rho}{\rho_0}\right)^{\gamma-1} \mathrm{e}^{-(\gamma-1)[(a\rho_0^{b-1})/(b-1)][1-(\rho/\rho_0)^{b-1}]}. \tag{17}$$

From (11), it can be concluded that because the internal energy remains unchanged after the gas expansion, the temperature would remain constant

$$T = T_0 \rightarrow \frac{P}{R(\rho + a\rho^b)} = \frac{P_0}{R(\rho_0 + a\rho_0^b)} \tag{18}$$

and

$$\frac{P}{P_0} = \frac{(\rho + a\rho^b)}{(\rho_0 + a\rho_0^b)}. \tag{19}$$

Then from (17),

$$\begin{aligned}\frac{P}{P_0} &= \frac{\rho}{\rho_0}\frac{1 + a\rho_0^{b-1}(\rho/\rho_0)^{b-1}}{1 + a\,\rho_0^{b-1}}\frac{T}{T_0}\\ &= \frac{\rho}{\rho_0}\frac{1 + a\rho_0^{b-1}(\rho/\rho_0)^{b-1}}{1 + a\rho_0^{b-1}}\left(\frac{\rho}{\rho_0}\right)^{\gamma-1}\\ &\quad\times \mathrm{e}^{-(\gamma-1)[(a\rho_0^{b-1})/(b-1)][1-(\rho/\rho_0)^{b-1}]}.\end{aligned} \tag{20}$$

3.3. Frictional uniform gas flow

To include the effects of wall friction on gas flow, a simple friction law is considered [23]:

$$f = \frac{8\tau_w}{\rho V^2}, \tag{21}$$

where f is usually defined from the Reynold's number and the relative smoothness of the wall. As a special case, a circular cross section is assumed. It will also be used as an initial estimate for the non-uniform flow model

$$\begin{aligned} &l = 2\pi r,\\ &A = \pi r^2,\\ &\frac{l}{A} = \frac{2\pi r}{\pi r^2} = \frac{2}{r} = \frac{4}{D}\end{aligned} \tag{22}$$

and following (11)

$$u = C_V T = \frac{R}{\gamma - 1}T = \frac{1}{\gamma - 1}\frac{P}{\rho} \tag{23}$$

simplified versions of Eqs. (6)–(8) can be derived in terms of the Mach number M,

$$M^2 = \frac{V^2}{c^2} = \frac{\rho V^2}{\gamma P} = \frac{V^2}{\gamma RT} \tag{24}$$

so

$$\frac{\mathrm{d}\rho}{\mathrm{d}x} = \frac{f\rho M^2}{2D}\frac{\gamma}{(M^2 - 1)}, \tag{25-1}$$

$$\frac{\mathrm{d}V}{\mathrm{d}x} = -\frac{fM^2 V}{2D}\frac{\gamma}{(M^2 - 1)}, \tag{25-2}$$

$$\frac{\mathrm{d}P}{\mathrm{d}x} = \frac{f\rho V^2}{2D}\frac{1 + M^2(\gamma - 1)}{(M^2 - 1)}. \tag{25-3}$$

From derivative of (24)

$$\frac{\mathrm{d}M^2}{\mathrm{d}x} = \frac{V^2}{\gamma P}\frac{\mathrm{d}\rho}{\mathrm{d}x} + \frac{2\rho V}{\gamma P}\frac{\mathrm{d}V}{\mathrm{d}x} - \frac{\rho V^2}{\gamma P^2}\frac{\mathrm{d}P}{\mathrm{d}x} \tag{26}$$

results in the following differential equation:

$$\frac{(1-M^2)\,\mathrm{d}M^2}{\gamma(M^2)^2[1+M^2((\gamma-1)/2)]} = f\,\frac{\mathrm{d}x}{D}. \tag{27}$$

Integrating (27) from 0 to L (points 1 and 2) results in

$$\frac{1}{\gamma}\left(\frac{1}{M_1^2}-\frac{1}{M_2^2}\right)+\frac{1}{2}\left(\frac{\gamma+1}{\gamma}\right) \times \ln\left[\left(\frac{M_1}{M_2}\right)^2\frac{2+(\gamma-1)M_2^2}{2+(\gamma-1)M_1^2}\right]-\frac{fL}{D}=0. \tag{28}$$

3.4. Non-uniform isentropic gas flow

To further extend the formulation, a non-uniform isentropic gas flow model is now developed. For the sake of simplicity, only non-frictional steady flow within a duct with continuously changing geometry is presented [23]:

$$q_{\mathrm{w}} = \tau_{\mathrm{w}} = 0. \tag{29}$$

Equations of mass, momentum and energy conservation (3) can then be modified to

$$\frac{\mathrm{d}}{\mathrm{d}x}(\rho V A) = 0, \tag{30}$$

$$\frac{\mathrm{d}}{\mathrm{d}x}(\rho V^2 + P) = 0, \tag{31}$$

$$\frac{\mathrm{d}}{\mathrm{d}x}\left(u + \frac{V^2}{2} + \frac{P}{\rho}\right) = 0. \tag{32}$$

Integrating Eq. (32), and defining $C_p = \mathrm{d}h/\mathrm{d}T = \gamma R/(\gamma-1)$, $h = u + P/\rho$, results in the following enthalpy equation for an ideal gas in terms of the conditions "$_0$" of rest ($u_0 \equiv 0$):

$$h - h_0 = C_p(T - T_0), \tag{33}$$

$$C_p(T - T_0) + \frac{V^2}{2} = 0 \tag{34}$$

which, after some manipulation can be written as

$$\frac{T_0}{T} = 1 + \frac{\gamma-1}{2}\frac{V^2}{\gamma RT} \tag{35}$$

or in terms of the Mach number,

$$\frac{T_0}{T} = 1 + \frac{\gamma-1}{2}M^2. \tag{36}$$

Therefore, for any two points 1 and 2 along the duct,

$$\frac{T_2}{T_1} = \frac{(T_0/T)_{\text{at point 1}}}{(T_0/T)_{\text{at point 2}}} = \frac{2+(\gamma-1)M_1^2}{2+(\gamma-1)M_2^2} \tag{37}$$

and

$$\frac{P_2}{P_1} = \frac{M_1}{M_2}\left[\frac{2+(\gamma-1)M_1^2}{2+(\gamma-1)M_2^2}\right]^{1/2}, \tag{38}$$

$$\frac{\rho_2}{\rho_1} = \frac{M_1}{M_2}\left[\frac{2+(\gamma-1)M_1^2}{2+(\gamma-1)M_2^2}\right]^{-1/2}. \tag{39}$$

Finally, the solution procedure for each gas flow in a typical conduit can be summarized as [23]

1. For the first stage where the gas simply expands to fill the assumed conduit volume, pressure P_0, density ρ_0 and temperature T_0 are determined from the EOS equation (13).
2. Pressure P_1, density ρ_1 and temperature T_1 are determined from Eqs. (18)–(20) for the second stage where both the gas and the chamber expand (isentropic expansion).
3. Non-uniform isentropic gas flow:
   (a) Use Eq. (28) with $f = 0$ to evaluate M_2. A numerical approach may be required.
   (b) Use Eqs. (37)–(39) to evaluate P_2, ρ_2 and T_2 from P_1, ρ_1 and T_1.
4. Corrections if there exists some mass transfer out of the system:
   (a) If $|P_2 - P_{\mathrm{atm}}|/P_{\mathrm{atm}} < \varepsilon$, GOTO 5.
   (b) Assume a new mach number M_2.
   (c) Use Eq. (28) with $f = 0$ to predict M_1. A numerical solution may be required.
   (d) Use Eqs. (37)–(39) to evaluate P_2, ρ_2 and T_2 from P_1, ρ_1 and T_1.
   (e) GOTO 4(a).
5. GOTO the next conduit.

Complex 2D spatial problems are simplified to coupled evolving 1D flow analyses. The 2D solution procedure consists of several 1D analysis of gas flow in each duct (crack or opening). Crack lengths and openings are determined from the finite/discrete element solution of the solid domain.

4. Numerical verification

4.1. Example 1

In this example, an explosion occurs inside a solid chamber and effects of gas flow and variations of the gas pressure are investigated. Experimental results are available for this simple example, which can be used to verify the algorithm of calculating variations of gas pressure due to its escape from the open end of the chamber. The rigid chamber is built of a metal cylinder of length 1220 mm and diameter 25.4 mm as depicted in Fig. 5. The chamber is filled with $m = 0.148$ kg ANFO explosive material with an initial density $\rho = 240\,\mathrm{kg/m^3}$. The velocity of detonation (VOD) is assumed to be 1725 m/s and the process releases a gas with 3700 kJ/kg energy.

The analysis is performed by the assumption that the whole explosive material is detonated at once. As a result, the internal

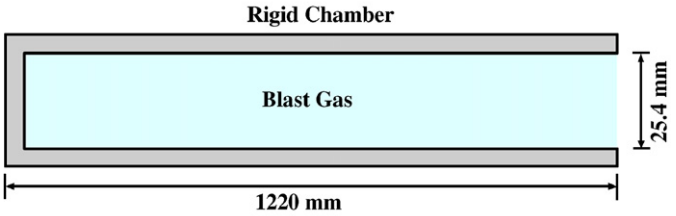

Fig. 5. Geometry of the rigid chamber.

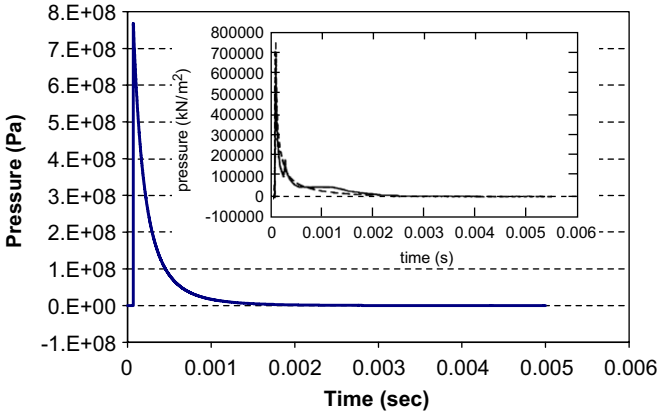

Fig. 6. Variations of pressure in comparison to the experimental results [16].

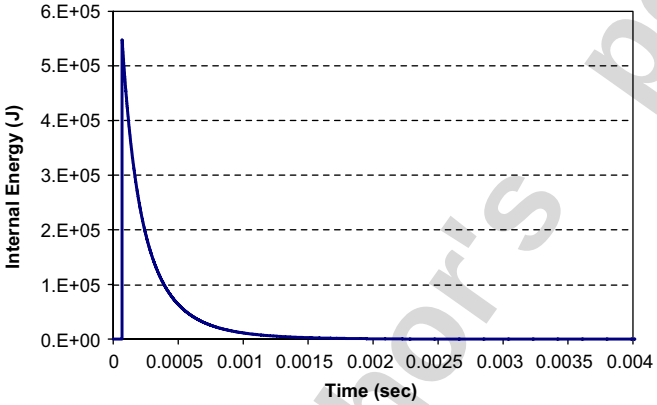

Fig. 7. Variations of internal energy for the second approach.

pressure is suddenly increased to a maximum value. The gas starts to escape from the chamber immediately after the detonation, resulting in sharp decreases in mass, pressure, density and internal energy (Figs. 6–9). Trend of variation and the peak pressure are in good agreement with available experimental results and the approach proposed by [16] (Fig. 6).

4.2. Example 2

The second example is to simulate a simple bullet firing test in order to verify the proposed algorithm of interaction of gas

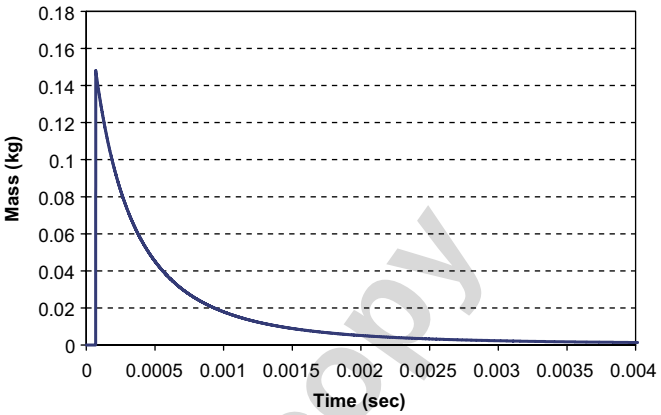

Fig. 8. Variations of mass for the second approach.

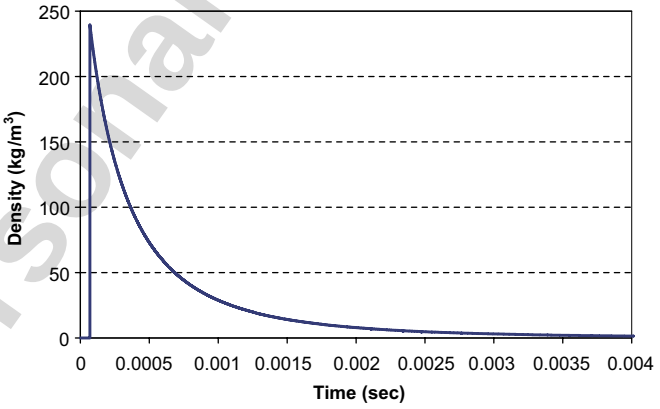

Fig. 9. Variations of density for the second approach.

with a changing volume. Such an experiment is basically performed to assess and compare measures of explosive materials, where a certain bullet with assumed geometry and mass is fired by the detonation of a specified mass of explosive material. The experiment is repeated for various masses of explosive material, and the maximum velocity and kinetic energy of the bullet are measured resulting in design diagrams.

This test is considered here to verify the interaction of the gas with its changing surrounding medium while leaving the firing container (a variable volume system).

The firing gun, as depicted in Fig. 10, consists of two compartments: one for the bullet and the other for the explosive material. The volume of the explosive compartment is 295 cm^3 and the total volume is 1913 cm^3. The bullet mass is 18 kg. The explosive material is Nitro Glycerin with specifications according to Table 1. Three different masses of explosive material, as defined in Table 2, are assumed and the results of simulation are compared with the experimental results.

An axisymmetric model is constructed and a simple finite element mesh composed of 41 and 8 elements for the gun and bullet, respectively, is used for modeling the problem (Fig. 11).

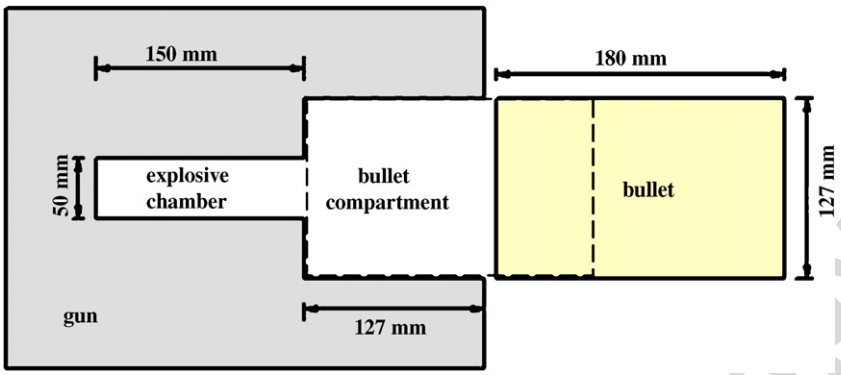

Fig. 10. A simple projectile firing system.

Table 1
Properties of the explosive material

T_{exp}	Q_{exp}	γ	a	b
4920 kg	6280e3 J	1.15	10.99e − 10	4.0

Table 2
Specifications of blast, velocity and kinetic energy of the bullet for three different masses of explosives

$M_e(g)$	ρ_{exp} (kg/m^3)	P_{exp} (Pa)	V_{max} (m/s)	$E_{C\,max}$ (kN m)
5.0	16.9	6.62×10^7	30.6	8.44
10.0	33.9	4.41×10^7	43.3	16.88
15.0	50.8	2.20×10^7	53.1	25.35

By detonation of the explosive material, a mixture of gas with high pressure and temperature is produced. Under this pressure, the bullet is accelerated from its resting position (Fig. 11). By advancing the bullet forward, the gas expands and fills the space behind the bullet. By expansion and propagation of the gas, density, pressure and internal energy are reduced. The process is followed until the bullet leaves its compartment.

The volume increase is proportional to the bullet velocity. According to Figs. 12–15, although the acceleration is high at the early stages of explosion, nevertheless, the velocity is low and the rate of reduction of pressure, density and energy remain low. However, by increasing velocity (and decreasing acceleration), the rate of volume increase and then the rate of reduction of density, pressure and internal energy of gas are increased; depicted by higher negative slopes.

The largest portion of the pressure on the bullet is induced immediately after the detonation. This pressure is reduced as the bullet advances outwards with an increasing velocity (Fig. 16).

When the bullet is about to leave its compartment, the system volume reaches its final value. At the same time, density and pressure are greatly reduced. It is to be noted that in contrary to pressure and density, the internal energy of the system remains almost unchanged from the detonation until the bullet leaves the gun (Fig. 13). Another important point that confirms the proposed algorithm is that the mass of gas remains constant until the bullet leaves the gun (Fig. 14).

A sudden drop in system mass is observed as the bullet leaves the gun (Fig. 14). As a result of rapid mass reduction, pressure, density and the internal energy are similarly reduced, causing a sudden change in slope. Finally, all curves converge to the time axis (zero value). At this stage, the bullet undergoes no further acceleration, and it continues to travel with the same velocity (Figs. 16 and 17).

Finally, Fig. 18 depicts the maximum kinetic energy of the bullet for different amounts of explosive mass, which shows a very good agreement with available experimental results [5].

An interesting point can be made by qualitatively comparing the results of this example and the previous one. The first example showed faster reduction rates for density, pressure and internal energy than the present example. The reason is that the process of gas escape in the first example started immediately after the completion of the explosion process. This results in a very fast departure of high pressure and density gas, which causes fast reduction in density, pressure and internal energy. In contrary, in the second example, reductions in density, pressure and internal energy before the bullet exits are only related to the gas expansion within the system, because no mass leaves the system.

4.3. Example 3

The final example simulates and discusses the fracture and fragmentation of a square concrete block. The concrete block is a $2 \times 2\,m^2$ with a unit thickness of 1 m, modeled as a 2D plane strain problem as depicted in Fig. 19. A narrow 1 m height and 1 cm width borehole exists in the middle of the block. The combined finite/discrete element approach is used to simulate the fracture and fragmentation process of the solid material subjected to extensive detonation gas pressure. Fully nonlinear frictional contact algorithms and large deformation procedures

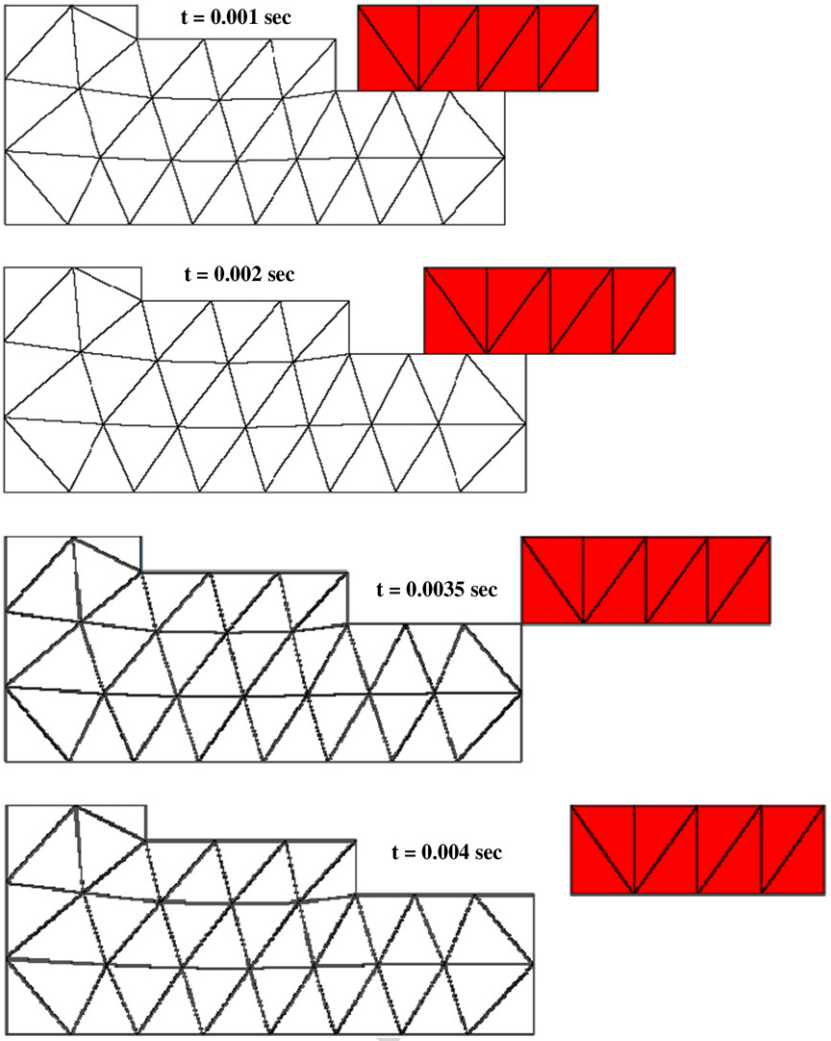

Fig. 11. Projectile (shaded) locations at different times ($M_e = 0.015$ kg).

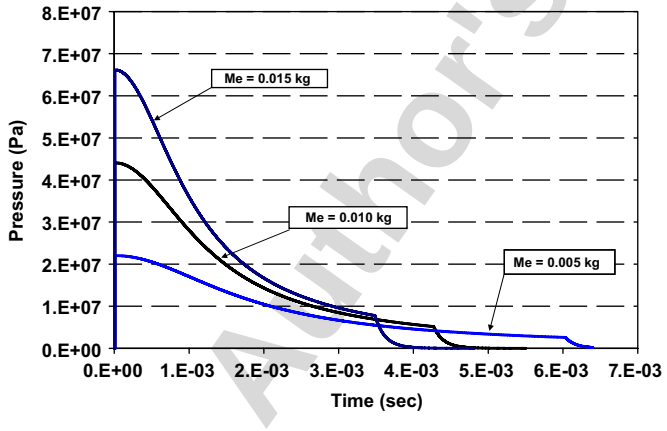

Fig. 12. Pressure of gas within the gun for different values of M_e.

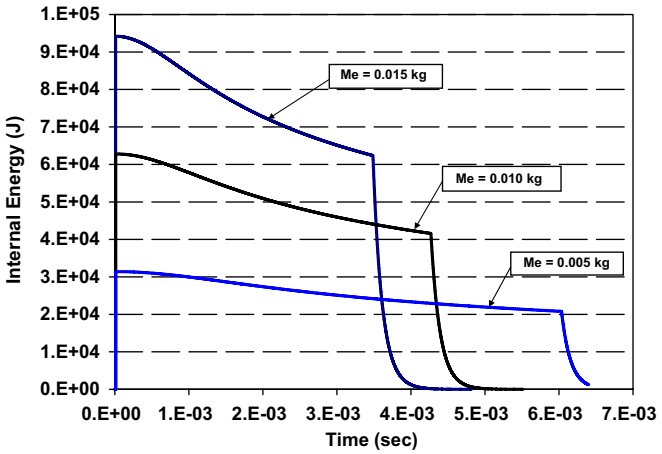

Fig. 13. Internal energy of gas within the gun for different values of M_e.

are embedded within the finite/discrete element methodology to evaluate and update stress states. The Rankine bilinear softening model [15] is assumed to govern the cracking behavior of the solid material. Re-meshing algorithms are also adopted for geometric modeling of cracks and fragments. The necessary parameters including the elastic modulus E, fracture energy

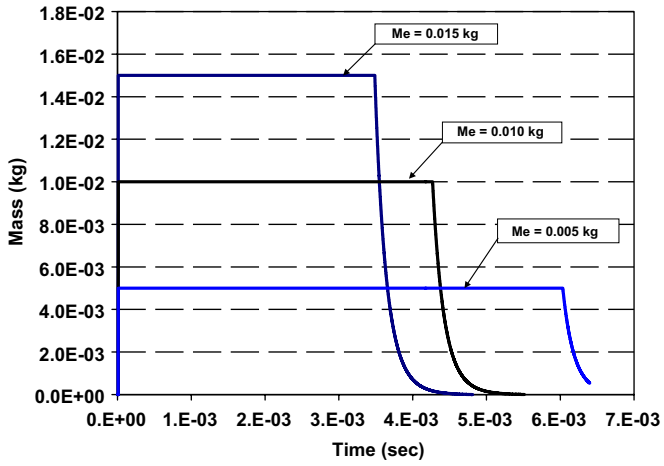

Fig. 14. Mass of gas within the gun for different values of M_e.

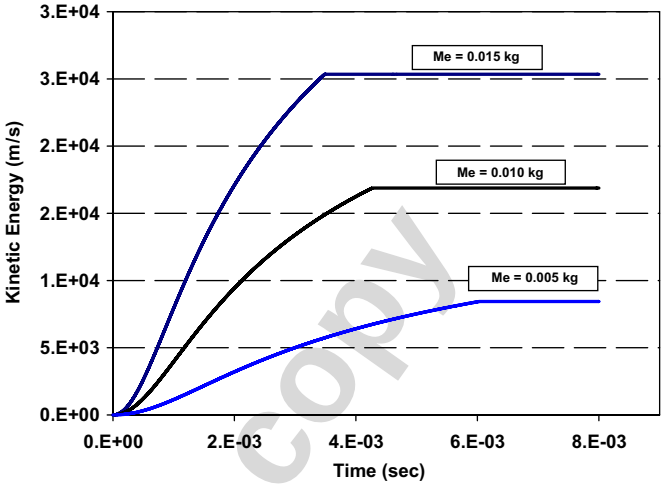

Fig. 17. Variations of projectile kinetic energy.

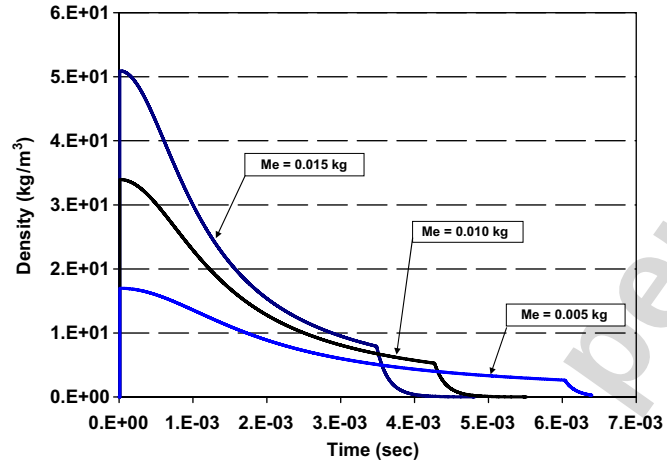

Fig. 15. Density of gas within the gun for different values of M_e.

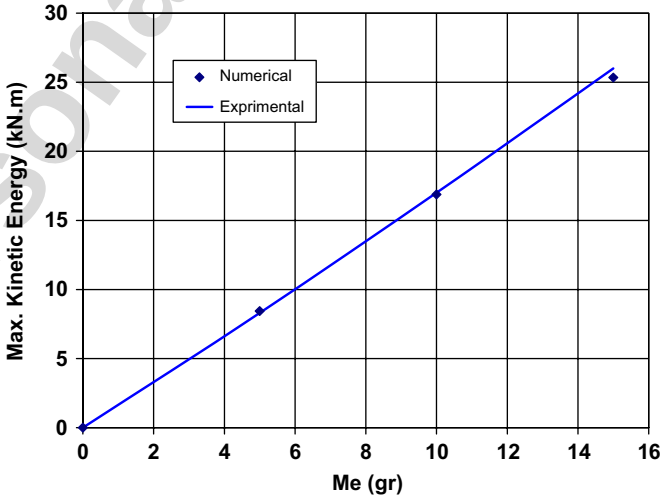

Fig. 18. Kinetic energy of the projectile for different explosive masses in comparison to the experimental results [5].

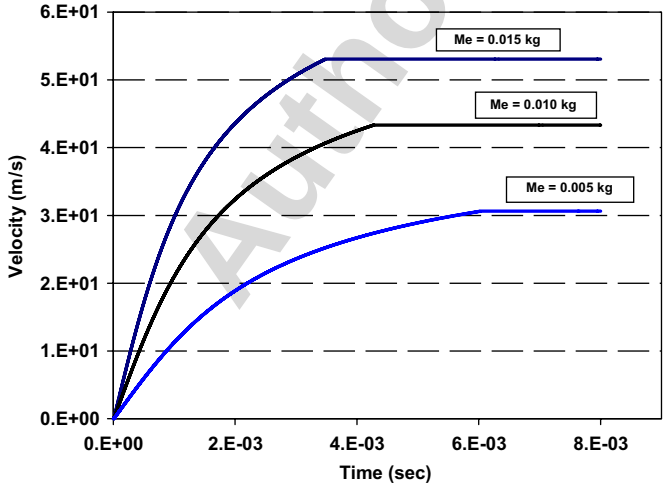

Fig. 16. Variations of projectile velocity.

release rate G_f and the maximum tensile strength f_t are taken similar to un-reinforced concrete properties (Table 3).

An unstructured finite element mesh with 4535 linear triangular elements is used for modeling the concrete block (Fig. 20). Finer finite elements are used around the borehole to ensure the necessary quality of the finite element solution.

The explosive material is filled from the bottom of the borehole to a 0.526 m height. The EOS for the explosive material, Nitro Glycerin, is assumed to follow the $P = (\rho + a\rho^b)RT$ equation, with the parameters defined in Table 4.

The gas effective region, illustrated in Fig. 19, is defined based on various parameters, such as the initial pressure of the gas produced from the explosion, the mass of explosive material, geometry of the borehole, etc. Further study is required to effectively determine the geometry of this region for general blast problems.

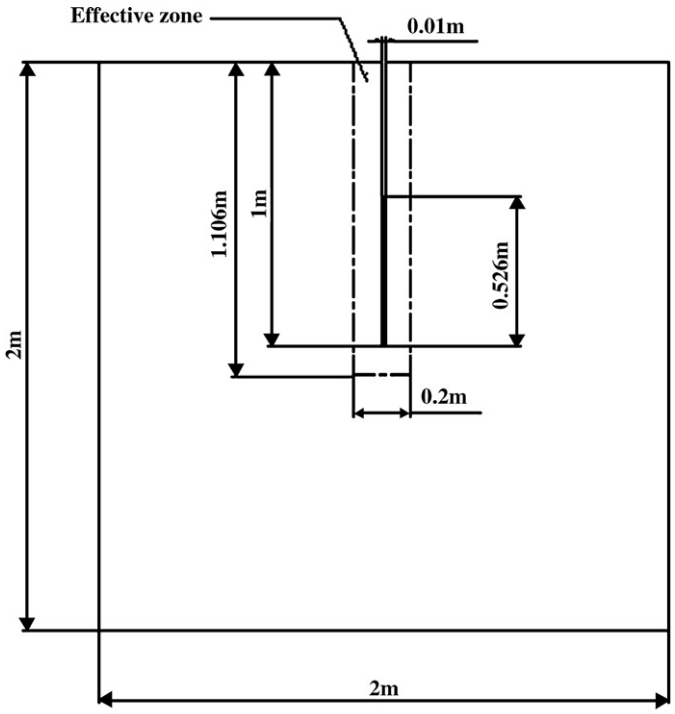

Fig. 19. Geometry of the concrete block.

Table 3
Mechanical properties of concrete

E	ν	f_t	G_f	ρ
2×10^{10} N/m^2	0.1	1×10^6 N/m^2	110 N m	2400 kg/m^3

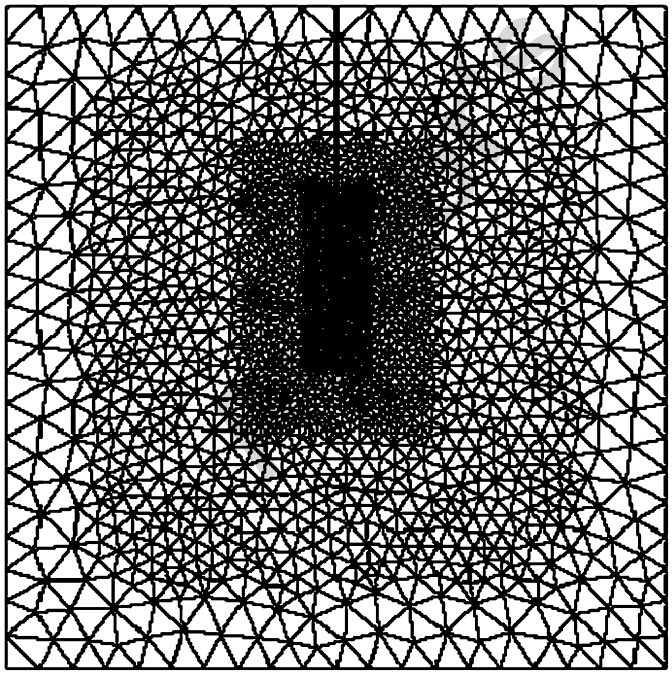

Fig. 20. Finite element mesh for the concrete block.

Table 4
Properties of the explosive material

M_{exp} (kg)	ρ_{exp} (kg/m^3)	P_{exp} (GPa)	T_{exp} (K)
8.416	1600	10.0	3300
VOD (m/s)	γ	a	b
7580	1.15	10.99e − 10	4.0

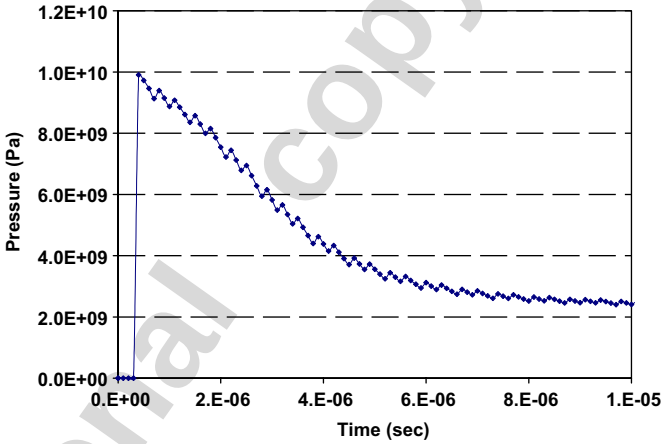

Fig. 21. Borehole pressure during the detonation of explosion cells.

In order to model the explosion process, the explosive material column is divided into smaller parts, called the explosion cells. The number and geometry of these cells depend mainly to the size of the finite element mesh in this region and the length of the explosion column. In the present example, the column of the explosive material has been divided into 400 equal cells. Detonation of the first cell, results in advancing the detonation and explosion phenomena within the explosion column with a velocity of 7580 m/s. Pressure of the induced gases at the explosion front is equal to the initial pressure of the explosion. In another words, a pressure equivalent to 10.0 GPa is applied to the borehole sides by detonation of each cell. Such an intensive pressure, results in expansion of the borehole volume and creation of cracks and fractures, which causes the expansion of explosion gas and a reduction in its initial pressure. The mechanical work done by the gas further reduces its internal energy.

By advancing the detonation of new cells, further pressure, equivalent to the initial pressure of 10.0 GPa, is applied to the borehole sides. The deformation and creation of cracks from the detonation of previous cells reduce the pressure of the system, however, the overall pressure of the system is increased due to the propagation of the gas through the complex geometry of the cracked medium and its mixture by already created gases from detonation of previous cells. Fig. 21 illustrates variations of the pressure of the system during the initial stages of the explosion process. Remarkably fast pressure reduction trend can be attributed to the possibility of smooth gas escape from the borehole, comparable to the relatively slow pressure decrease in the previous example (Fig. 12) which

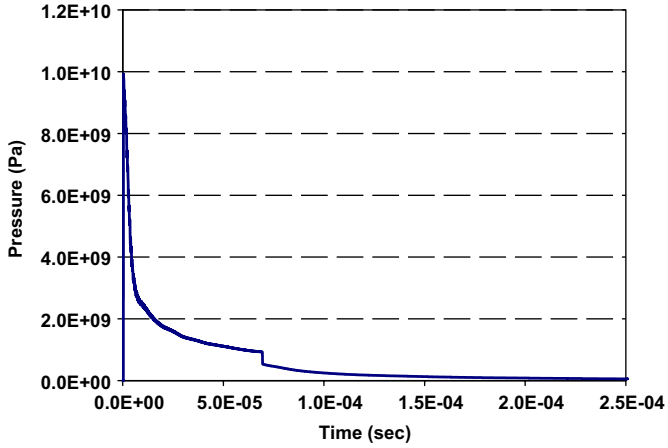

Fig. 22. Variations of pressure within the borehole.

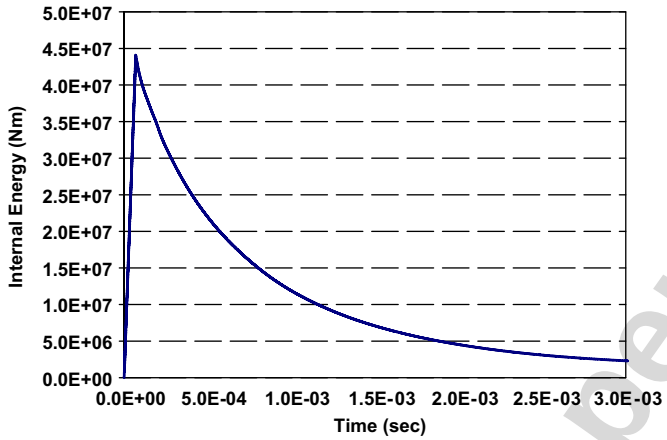

Fig. 23. Variations of internal energy within the borehole.

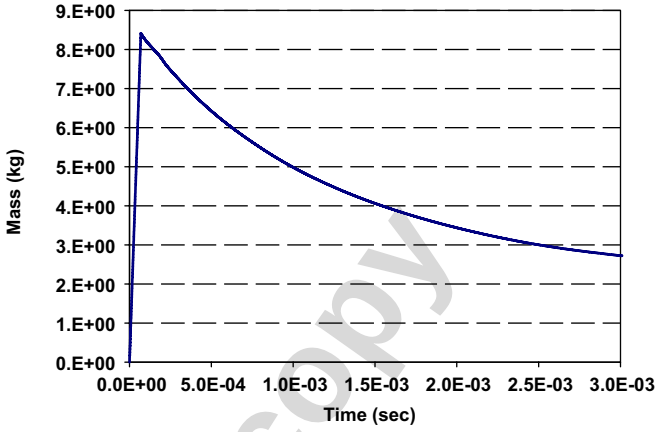

Fig. 24. Variations of mass within the borehole.

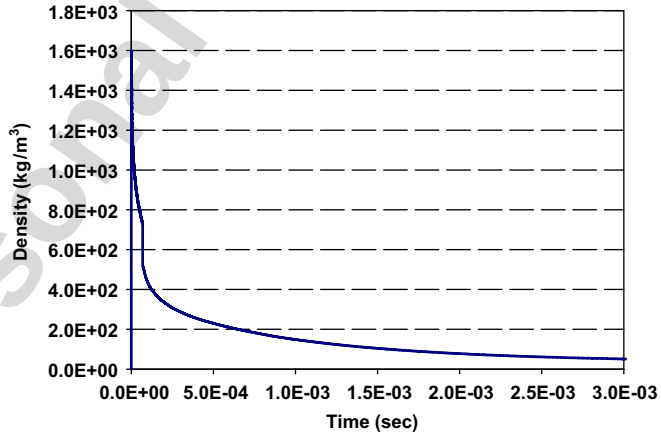

Fig. 25. Variations of density within the borehole.

was as a result of restriction by the relatively massive bullet movement.

According to this figure, after detonation of each cell, the system pressure is reduced due to induced deformation and cracking. However, it increases immediately after detonation of a new cell, and the same pattern is repeated until the end of detonation. It is also observed that the effect of high pressure gases created from detonation of new cells is decreased by the increase in deformation and cracking of the solid medium.

There is a difference between the borehole height (1 m) and the height of the explosive material (0.526 m). Therefore, by the end of the detonation process, the explosion-induced gases are suddenly propagated within the whole borehole space, causing a steep decrease in pressure (Fig. 22). Additionally, by increasing the extent of cracking to the boundaries of the gas effects, the gas may escape the effective region, further accelerating the reduction in density, pressure and internal energy of the gas, as illustrated in Figs. 22–25. A short time after the explosion, all curves converge to a small value.

Despite the reduction of gas pressure, fragments of the solid material continue to move following their acceleration, which results in further destruction of the top half of the block (Fig. 26a–f).

It is worth noting that although the whole process of explosion takes place in a very small time, it may have major effects on fracture and fragmentation patterns. This can be illustrated by comparing the pressure history and cracking patterns of the present method to the two-mesh model given in [15] (Figs. 27–29).

Ref. [15] assumed that any interaction between the gas and deformation of the cracked media would be enforced only after the end of blast reactions inside the borehole, keeping the borehole pressure a constant equal to the initial gas pressure. This has two adverse effects; one is being physically unrealistic, and the other is its excessive deformation of the borehole, while ignoring its effects on pressure and other thermo-mechanic quantities. According to Fig. 27 the pressure suddenly reduces to a value much lower than the initial blast pressure (10.0 GPa). This may cause a sudden negative effect on borehole sides causing extensive cracking and falling the fragments inside the borehole (Fig. 29). This phenomenon is expected to be less important for explosive material with lower initial pressures.

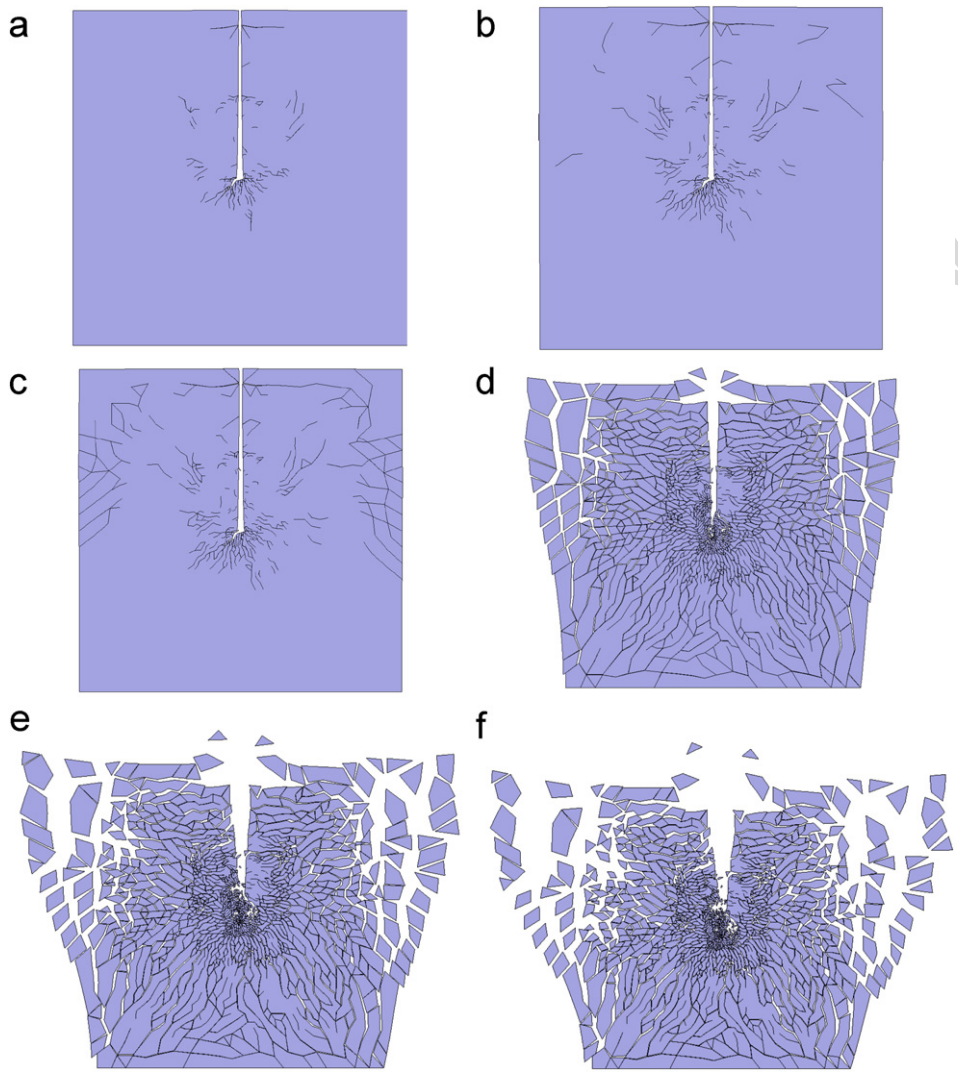

Fig. 26. Cracking patterns at different times. (a) $t = 0.0003$ s, (b) $t = 0.0005$ s, (c) $t = 0.00055$ s, (d) $t = 0.005$ s, (e) $t = 0.01$ s, (f) $t = 0.015$ s.

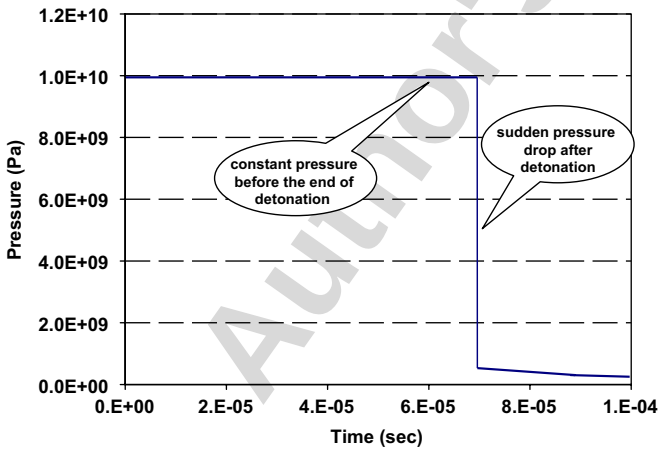

Fig. 27. Borehole pressure according to the algorithm of [15].

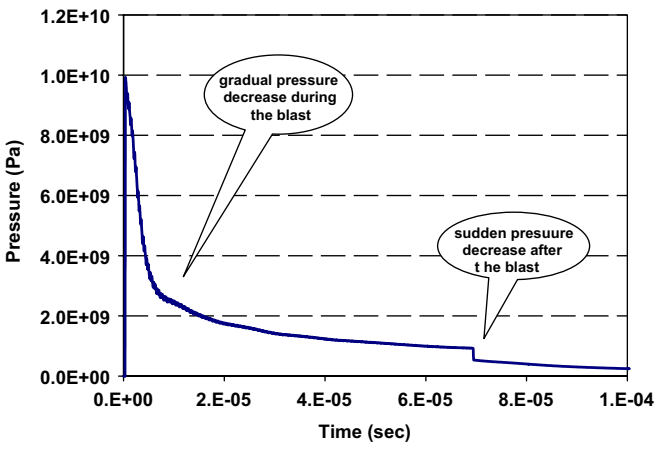

Fig. 28. Borehole pressure according to the proposed algorithm.

Fig. 28 illustrates the rapid pressure reduction predicted by the proposed approach. A small sudden reduction in the middle of the curve is associated to the time of full detonation. At this time the reduction in pressure due to gas expansion is no longer accompanied by new cell detonations. As a result, a sudden drop in pressure is anticipated.

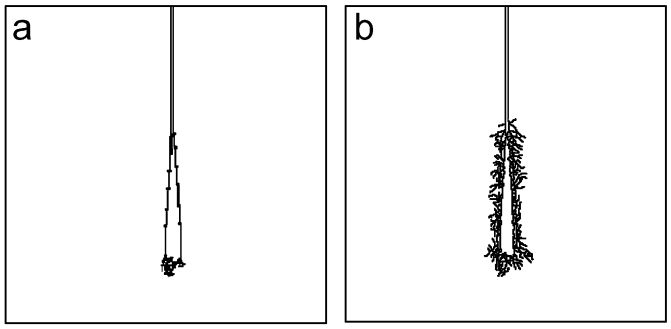

Fig. 29. Blast-induced cracking patterns. (a) Algorithm of [15], (b) present algorithm.

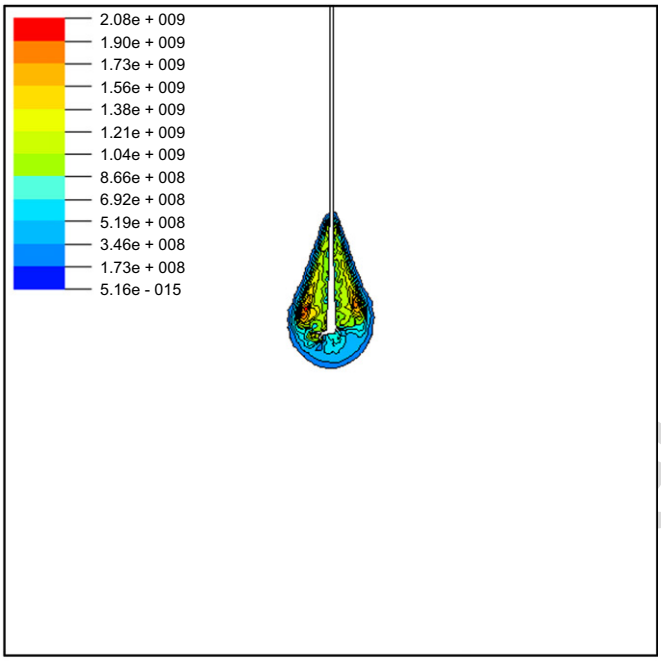

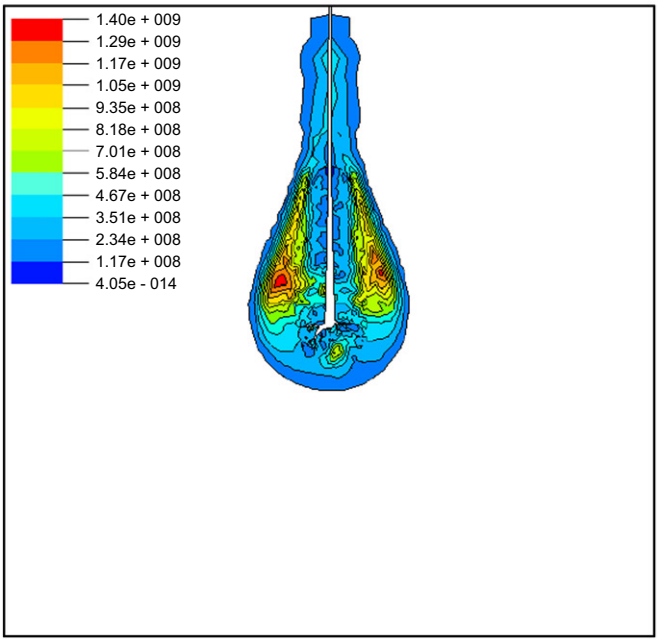

Fig. 30. Effective stress contours at $t = 0.00005$, 0.0001 s.

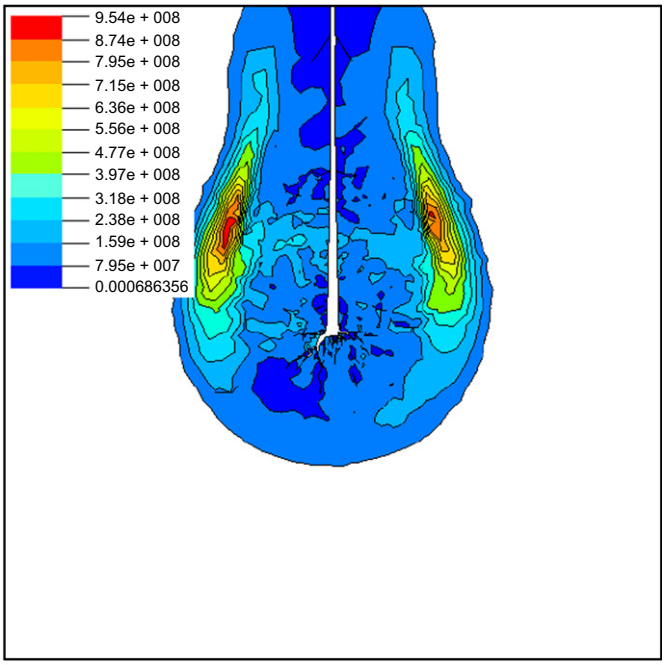

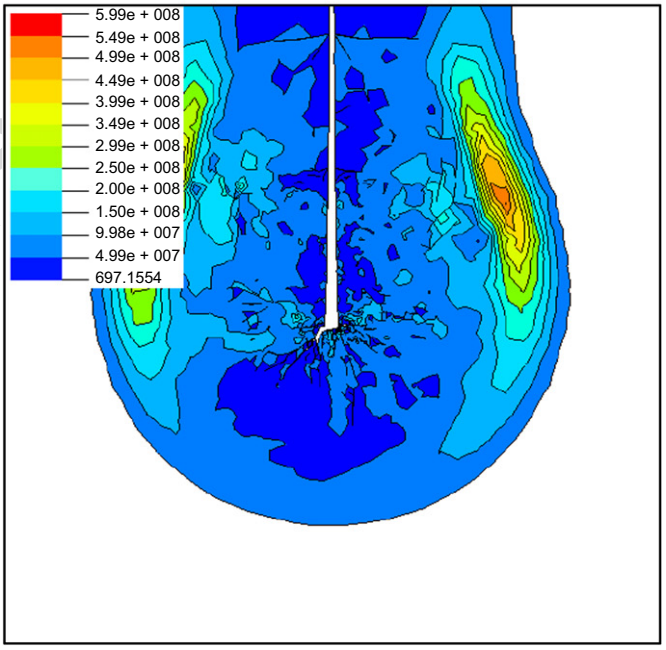

Fig. 31. Effective stress contours at $t = 0.0002$, 0.0003 s.

The final point which has to be mentioned is the way the fracture pattern is affected by the solid material model. According to Figs. 30–32, compressive stress waves are propagated outwards as a front. However, the Rankine strain softening model assumes a measure of tensile stresses or stains as the governing measure of cracking. Therefore, for the present problem, crack initiation and propagation cannot be appropriately modeled around the borehole at initial stages. Afterwards, however, by propagation of the compressive stress waves and their reflection from free edges (Fig. 30), the resultant tensile stress waves may satisfy the Rankine tensile crack criterion, causing extensive cracking at free edges of the block. For a more

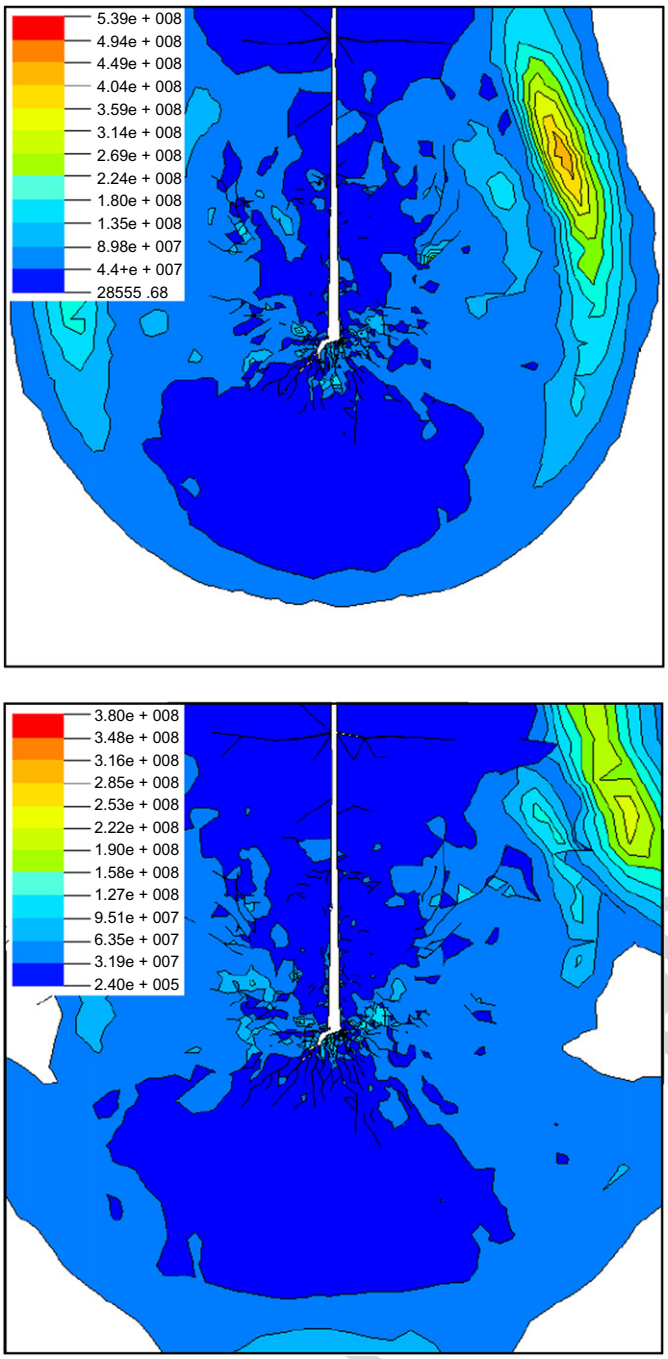

Fig. 32. Effective stress contours at $t = 0.0004,\ 0.0005$ s.

realistic modeling of practical problems, a more sophisticated material behavior, capable of modeling both tensile and compressive failure modes, has to be adopted.

5. Conclusion

A non-uniform isentropic gas flow model coupled with solid mechanics is developed and implemented into a combined finite/discrete element methodology to simulate the complex behavior of explosions that cause extensive fracture and fragmentation within a solid. The cracking and deformation affects the pressure and density of the gas induced by blast; a full coupling phenomenon. Numerical simulations have shown good agreement with available benchmarks. Compared to other sophisticated gas–solid interaction models, the proposed approach avoids using an independent finite element mesh for solving the gas flow equations which greatly simplifies the overall solution and the numerical simulation.

References

[1] A.A. Bauer, D. Fratzos, Finite element modeling of pre-split blasting using measured time curves, in: Society of Explosive Engineers Annual Meeting, Miami, USA, 1987.
[2] D.L. Chapman, On the rate of explosion in gases, Philos. Mag. 213, Series 5 (47) (1899) 90.
[3] E. Joughet, Sur la propagation des reactions chiiques dans la gaze, J. Pure Appl. Math. 70, Series 6 (1) (1905) 347.
[4] R.E. Danell, T. Lewnardowski, V.K. Laun Mai, Influence of discontinuities on pre-splitting effectiveness, Int. J. Blasting Fragmentation 1 (1997) 27–41.
[5] C.H. Johnsson, P.A. Persson, Detonics of High Explosives, Academic Press, London, UK, 1970.
[6] A. Munjiza, Discrete elements in transient dynamics of fractured media, Ph.D. Thesis, University of Wales Swansea, 1992.
[7] L. Xian, N. Bicanic, D.R.J. Owen, A. Munjiza, Rock blasting simulation by rigid body dynamic analysis and rigid brittle fracturing model, in: Proceedings of the International Conference on Nonlinear Engineering Computations, NEC-91, Pineridge Press, Swansea, UK, 1991, pp. 477–587.
[8] D.S. Preece, S.L. Burchell, D.S. Scovira, Coupled gas flow and rock motion modeling with comparison to bench blast field data, in: Proceeding Fragblast, vol. 4, 1993, pp. 239–247.
[9] A. Munjiza, D.R.J. Owen, N. Bicanic, A combined finite–discrete element method in transient dynamics of fracturing solids, Int. J. Eng. Comput. 12 (1995) 145–174.
[10] R.H. Nilson, An integral method for predicting hydraulic fracture propagation driven by gases or liquids, Int. J. Rock Mech. 22 (1996) 3–19.
[11] D.S. Preece, B.J. Thorne, A study of detonation timing and fragmentation using 3D finite element techniques and damage constitutive model, in: Proceeding Fragblast, vol. 5, 1996, pp. 147–156.
[12] A. Daehnke, H. Rossmanith, J.F. Schatz, On dynamic gas pressure induced fracturing, Int. J. Blasting Fragmentation 1 (1997) 59–73.
[13] P.A. Persson, The relationship between stain energy, rock damage, fragmentation and throw in rock blasting, Int. J. Blasting Fragmentation 1 (1997) 73–99.
[14] A. Minchinton, P. Lynch, Fragmentation and have modeling using coupled discrete element gas flow code, Int. J. Blasting Fragmentation 1 (1997) 49–59.
[15] S. Mohammadi, A. Bebamzadeh, A coupled gas–solid interaction model for FE/DE simulation of explosion, Finite Elem. Anal. Design 41 (2005) 1289–1308.
[16] A. Munjiza, J.P. Latham, K.F. Andrews, Detonation gas model for combined finite-discrete element simulation of fracture and fragmentation, Int. J. Numer. Methods Eng. 49 (2000) 1495–1520.
[17] A. Munjiza, K.R.F. Andrews, J.K. White, Combined single and smeared crack model in combined finite–discrete element method, Int. J. Numer. Methods Eng. 44 (1998) 41–57.
[18] S. Mohammadi, Discontinuum Mechanics Using Finite and Discrete Elements, WIT Press, UK, 2003.
[19] A. Munjiza, The Combined Finite–Discrete Element Method, Wiley, UK, 2005.
[20] R.W. Lewis, B.A. Schrefeler, The Finite Element Method in the Static and Dynamic Deformation and Consolidation of Porous Media, second ed., England, 1998.

[21] S. Mohammadi, A. Pooladi, Unstructured two-mesh gas–solid interaction modeling of explosion in fractured solid media, 2006, submitted for publication.
[22] J.M. Powers, Lecture Notes on Gas Dynamics, Department of Aerospace and Mechanical Engineering, University of Notre Dame, 2003.
[23] A. Pooladi, Analysis of explosion and gas–solid interaction in fractured solid media, M.Sc. Thesis, School of Civil Engineering, University of Tehran, 2005.